Available online at www.sciencedirect.com
ScienceDirect
Bioorganic & Medicinal Chemistry Letters
Bioorganic & Medicinal Chemistry Letters 17 (2007) 5300–5309

The discovery of 6-amino nicotinamides as potent and selective histone deacetylase inhibitors

Christopher L. Hamblett,[a,*] Joey L. Methot,[a] Dawn M. Mampreian,[a] David L. Sloman,[a] Matthew G. Stanton,[a] Astrid M. Kral,[b] Judith C. Fleming,[b] Jonathan C. Cruz,[c] Melissa Chenard,[c] Nicole Ozerova,[b] Anna M. Hitz,[b] Hongmei Wang,[b] Sujal V. Deshmukh,[d] Naim Nazef,[d] Andreas Harsch,[d] Bethany Hughes,[e] William K. Dahlberg,[e] Alex A. Szewczak,[e] Richard E. Middleton,[e] Ralph T. Mosley,[f] J. Paul Secrist[b] and Thomas A. Miller[a]

[a]*Department of Drug Design and Optimization—Medicinal Chemistry, Merck Research Laboratories, 33 Avenue Louis Pasteur, Boston, MA 02115, USA*
[b]*Department of Cancer Biology and Therapeutics, Merck Research Laboratories, 33 Avenue Louis Pasteur, Boston, MA 02115, USA*
[c]*Department of Pharmacology, Merck Research Laboratories, 33 Avenue Louis Pasteur, Boston, MA 02115, USA*
[d]*Department of Drug Design and Optimization—Drug Metabolism and Pharmacokinetics, Merck Research Laboratories, 33 Avenue Louis Pasteur, Boston, MA 02115, USA*
[e]*Department of Drug Design and Optimization—Automated Lead Optimization, Merck Research Laboratories, 33 Avenue Louis Pasteur, Boston, MA 02115, USA*
[f]*Department of Medicinal Chemistry, Merck Research Laboratories, 126 Lincoln Avenue, PO Box 2000, Rahway, NJ 07065, USA*

Received 13 July 2007; revised 8 August 2007; accepted 13 August 2007
Available online 16 August 2007

Abstract—This communication highlights the development of a nicotinamide series of histone deacetylase inhibitors within the benzamide structural class. Extensive exploration around the nicotinamide core led to the discovery of a class I selective HDAC inhibitor that possesses excellent intrinsic and cell-based potency, acceptable ancillary pharmacology, favorable pharmacokinetics, sustained pharmacodynamics in vitro, and achieves in vivo efficacy in an HCT116 xenograft model.

Epigenetic defects alter levels of gene expression without structurally modifying DNA sequence and have been linked to the progression of a number of diseases, such as cancer.[1] In contrast to DNA mutations, epigenetic defects that lead to disease are potentially reversible by pharmacologically targeting the enzymes responsible for the epigenetic modifications.[2]

Histone acetylation is an epigenetic modification that is controlled by histone acetyltransferases (HATs) and histone deacetylases (HDACs).[3] Several HDAC inhibitors are currently in development as therapeutic agents and have been shown to regulate a variety of cellular responses including proliferation, differentiation, and apoptosis.[4] In general, inhibiting HDAC activity results in the accumulation of acetylated histones and subsequent activation of gene transcription.[5] Histone hyperacetylation induced by HDAC inhibitors has been shown to correlate with the anti-tumor effects of these inhibitors.[6] These observations suggest that HDAC inhibition provides an opportunity to reverse epigenetic defects that lead to disease and represents a promising new strategy for the treatment of cancer.

Class I and II histone deacetylases catalyze the removal of the acetyl group from the amino-terminal lysine residues of histones within nucleosomes.[7] While the biological functions of the many HDAC subtypes are still

Keywords: Epigenetics; Histone acetylation; Histone deacetylases; Nicotinamides; Benzamides.
* Corresponding author. Tel.: +1 617 992 2053; fax: +1 617 992 2043; e-mail: christopher_hamblett@merck.com

0960-894X/$ - see front matter © 2007 Elsevier Ltd. All rights reserved.
doi:10.1016/j.bmcl.2007.08.023

being defined, there is compelling evidence that class I HDACs regulate cell proliferation and therefore are viable targets for cancer therapeutics.[8]

Vorinostat (suberoylanilide hydroxamic acid, SAHA, Zolinza.™), a hydroxamate-based HDAC inhibitor, inhibits a subset of both class I and II HDAC enzymes and has recently been approved for marketing in the United States for the treatment of cutaneous manifestations of cutaneous T-cell lymphoma (Fig. 1).[9] More specifically, vorinostat inhibits HDACs 1, 2, 3, and 6 at the low nanomolar level (HDAC1 $IC_{50} < 0.1$ μM) while inhibiting HDAC8 and HDAC11 at the micromolar level.

A number of benzamide HDAC inhibitors, such as MS-275 (HDAC1 $IC_{50} > 1.0$ μM),[10] CI-994 (HDAC1 $IC_{50} > 100$ μM),[11] and MGCD-0103 (HDAC1 $IC_{50} \geqslant 0.1$ μM),[12] generally characterized as less potent HDAC inhibitors with greater class I selectivity compared to hydroxamate-based inhibitors, are under clinical investigation to further evaluate if they offer advantages to vorinostat with regard to efficacy and tolerability (Fig. 2).

Our medicinal chemistry efforts were initiated to discover an HDAC inhibitor with improved class I selectivity, greater tolerability, and improved efficacy compared to current inhibitors in development. Initial SAR focused on structural diversification around the pyridine core of nicotinamide lead **1**, which exhibits an HDAC inhibitory activity of 12.4 μM (Fig. 3).[13]

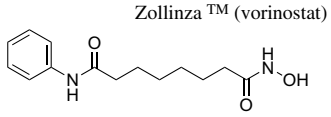

Figure 1. Vorinostat, a first in class hydroxamate-based HDAC inhibitor approved for the treatment of cutaneous T-cell lymphoma.

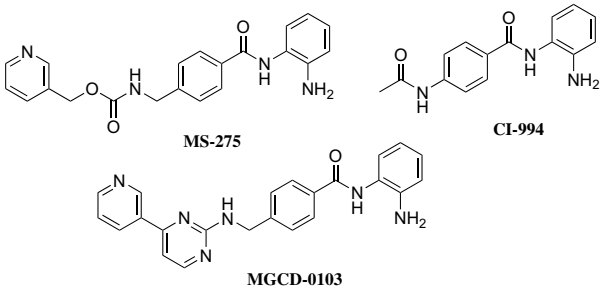

Figure 2. Representative benzamides under clinical evaluation.

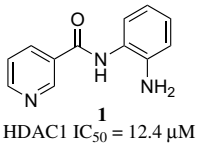

Figure 3. *N*-(2-Aminophenyl)nicotinamide (**1**) as a benzamide lead.

It was quickly determined that the 6-position of the pyridine ring could be easily functionalized and that derivatization with cyclic amines, such as *N*-substituted piperazines, led to a significant enhancement in HDAC inhibitory activity over analogs derived from corresponding acyclic amino derivatives. For example, acyclic dimethyl amine derivative **2** exhibited an HDAC inhibitory activity of 963 nM compared to piperazine **3** which was 168 nM (Table 1). In general, amino nicotinamide substitution with six-membered cyclic amines gave enhanced HDAC enzymatic activity compared to larger or smaller heterocyclic ring systems.

All nicotinamide analogs were prepared in excellent overall yields by either a linear 3- or 4-step sequence using one of two general methods: nicotinamides prepared by method A commenced with the acid chloride displacement of commercially available 6-chloronicotinoyl chloride with *t*-butyl (2-aminophenyl)carbamate **4**[14] to give the Boc-protected chloronicotinamide **5** in 84% yield. The sequence was completed by pyridyl chloride displacement in the presence of excess (3.0 equiv) functionalized (i) or unfunctionalized (ii) cyclic amine at 85 °C in DMSO. The piperazine was then further functionalized (ii) by acetylation, sulfonylation, or carbamoylation to give intermediate **6**, followed by TFA removal of the Boc group (i and ii) to afford the desired nicotinamide **7** (Scheme 1).

Nicotinamides prepared by method B began with the pyridyl chloride displacement of commercially available methyl 6-chloronicotinate with excess cyclic amine (3.0 equiv) to give intermediates **8**, followed by hydrolysis of the methyl ester with LiOH to give intermediates **9** and EDCI coupling in the presence of excess phenylenediamine to give the desired nicotinamide **7** by this alternative strategy (Scheme 2).

Having determined that 6-piperazinyl nicotinamides gave optimal HDAC inhibitory activity, we focused our efforts initially on modifications to the piperazine ring system by preparing a diverse set of analogs **7a**–**7m** (Table 2). For 6-piperazinyl nicotinamides lacking *N*-substitution where R^3 = H, no general trends emerged for enzymatic potency despite the structural and stereochemical modifications made on the piperazine ring

Table 1. Acyclic versus cyclic comparison at the 6-position

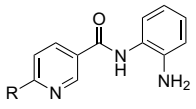

Compound	R	HDAC1 IC_{50} (nM)[a]
2	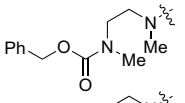	963
3	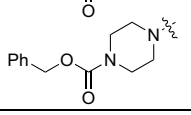	168

[a] Values are reported as an average for $n = 2$ or greater.

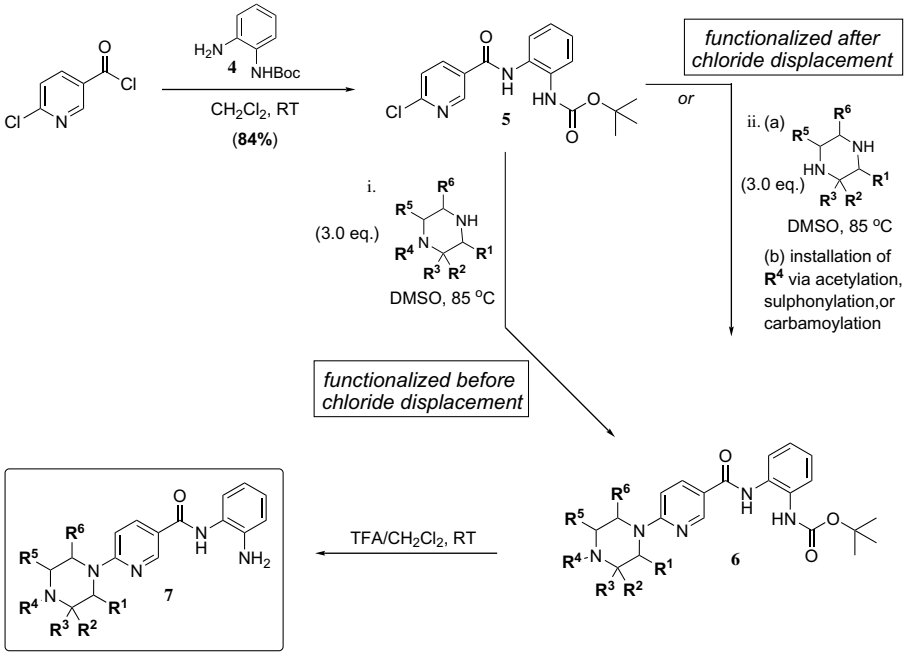

Scheme 1. Method A: general synthesis of *N*-(2-aminophenyl)-6-piperazinyl nicotinamides **7**.

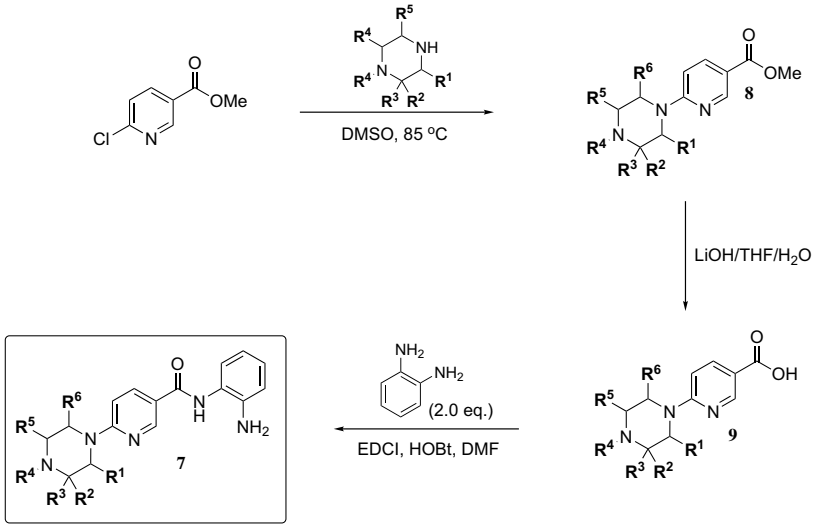

Scheme 2. Method B: alternative synthesis of *N*-(2-aminophenyl)-6-piperazinyl nicotinamides **7**.

system (**7a**–**7f**). The enzymatic activities for analogs **7a**–**7f** ranged from 301 nM (**7c**) to 821 nM (**7f**). The significance of the size and position of the substituents on the piperazine ring became clear when R^3 was further elaborated to a number of carbamate derivatives. Analogs with smaller R^1 and R^2 substituents, such as (*S*)-Me (**7g**, **7i**) or (*R*)-Me (**7j**), on the external 2-position of the piperazine were generally more potent than inhibitors with larger substituents, such as (*S*)-*i*-Pr (**7m**) and (*S*)-Bn (**7h**) when R^3 = Cbz or Boc. Analogs that contained disubstituted piperazines, such as dimethyl derivatives **7k** and **7l** with substituents either in the internal or external positions of the piperazine ring, were typically less potent than derivatives with mono-methyl substitution at the same positions when R^3 = Cbz. The two most potent inhibitors to emerge from the SAR were nicotinamides **7i** with an HDAC1 IC_{50} of 73 nM and **7j** with an HDAC1 IC_{50} of 40 nM.

The 6-amino nicotinamides were further evaluated in our cell-based HCT116 colon carcinoma growth inhibition[15] assay, which is a direct measure of in vitro antiproliferative effects, as well as an indirect measure of cell permeability. Several trends emerged from the cell-based results (Table 3). Inhibitors lacking *N*-substitution not only had poor intrinsic potency, but generally had poor cell-based potency as well as exemplified by **7a** with a GI_{50} of 1690 nM. Inhibitors with larger R^1/R^2 piperazine substituents, such as **7m** with R^1 = (*S*)-*i*-Pr, had a growth inhibition of 3484 nM, and inhibitors with

Table 2. HDAC1 activity for representative 6-piperazinyl nicotinamides

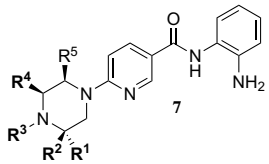

Compound	Method	R^1	R^2	R^3	R^4	R^5	HDACl IC_{50} (nM)[a]
7a	A[i]	(*S*)-*i*-Me	H	H	H	H	435
7b	A[i]	(*S*)-*i*-Pr	H	H	H	H	304
7c	A[i]	(*S*)-Bn	H	H	H	H	301
7d	A[i]	(*S*)-Me	H	H	H	(*R*)-Me	582
7e	A[i]	Me	Me	H	H	H	529
7f	A[i]	H	Me	H	Me	H	821
7g	B	Me	H	Boc	H	H	242
7h	B	Bn	H	Boc	H	H	352
7i	A[ii]	(*S*)-Me	H	Cbz	H	H	73
7j	A[ii]	H	(*R*)-Me	Cbz	H	H	40
7k	A[ii]	Me	Me	Cbz	H	H	169
7l	A[ii]	(*S*)-Me	H	Cbz	H	(*R*)-Me	255
7m	A[ii]	(*S*)-*i*-Pr	H	Cbz	H	H	326

[a] Values are reported as an average for $n = 2$ or greater.

Table 3. Enzymatic versus cell-based potency for representative nicotinamides

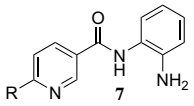

Compound	Method	R	HDAC1 IC_{50} (nM)[a]	HCT116-72h GI_{50} (nM)[a]	Shift in potency
7a	A[i]		435	1690	3.9
7g	B	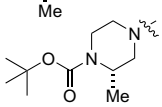	242	1100	4.5
7i	A[ii]	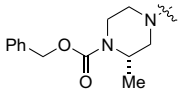	73	81	1.1
7j	A[ii]	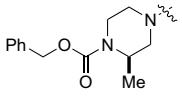	40	495	12.4
7k	A[ii]	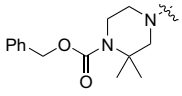	169	871	5.1
7l	A[ii]	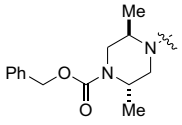	255	3317	13.0
7m	A[ii]	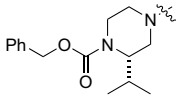	326	3484	10.7
7n	A[ii]	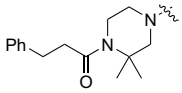	77	416	5.4
7o	A[ii]	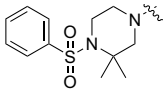	149	2435	16.3

[a] Values are reported as an average for $n = 2$ or greater.

Table 4. In vitro profile for representative urea analogs

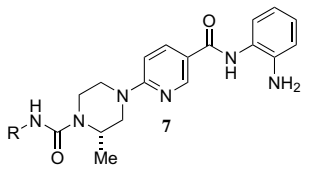

Compound	Method[a]	R	HDAC1 IC_{50} (nM)[b]	HCT116-72h GI_{50} (nM)[b]
7p	A[ii]	Ph	75	725
7q	A[ii]	Bn	39	916
7r	A[ii]	PMB	47	892
7s	A[ii]		101	1925
7t	A[ii]		47	902
7u	A[ii]		47	433

[a] Method A[i]: the ureas were prepared at room temperature using the functionalized piperazine nicotinamide, the corresponding isocyanate R—C=N=O (2.0 equiv) in DMF for up to 12 h.
[b] Values are reported as an average for $n = 2$ or greater.

disubstituted piperazines, such as dimethyl derivatives **7k** and **7l** with growth inhibitions of 871 and 3317 nM, respectively, generally had poor cell-based potencies and significant shifts from intrinsic potencies. *N*-sulfonamide derivatives also showed a dramatic shift from intrinsic potency to cell-based potency as demonstrated by dimethyl piperazine **7o** with a greater than 16-fold shift from HDAC inhibitory activity (149 nM) to HCT116 growth inhibition (2435 nM). Compounds that exhibited the greatest cellular potency contained small alkyl (R^1, R^2 = Me) mono-substituted piperazines coupled with CBz carbamates (R^3). The significance of chirality of the substituent in the distal 2-position (R^1/R^2) of the piperazine is most worthy of note. While **7j** with R^2 = (*R*)-Me possessed greater intrinsic potency (HDAC1 IC_{50} = 40 nM), **7i** with R^1 = (*S*)-methyl and an intrinsic potency of 73 nM gave a greater than 6-fold enhancement in cell-based potency (GI_{50} = 81 nM) over **7j** (GI_{50} = 495 nM).[16] While the mechanism for the remarkable 12-fold shift from HDAC enzymatic activity to cell-based potency for **7j** and other select 6-amino nicotinamides that exhibited this shift in potency is unclear, it may be attributable to an off-target cellular transport effect. The cell-based anti-proliferative effects of several analogs were further evaluated in vitro in HeLa cervical cancer cells. Nicotinamide **7i** displayed a remarkable cell-based potency with a GI_{50} of 28 nM.

Having identified that the (2*S*)-methyl piperazine moiety coupled with the Cbz carbamate functionality leads to an exceptional in vitro profile, we further evaluated a number of urea analogs **7p**–**7u** to determine if we could improve upon the potency and HCT116 growth inhibition of **7i** (Table 4). While a number of urea analogs showed comparable or slightly improved HDAC1 enzymatic potency compared to **7i** as exemplified by analogs **7p**–**7u** ranging in enzymatic activities from 39 nM (**7q**) to 101 nM (**7s**), none of the analogs achieved a GI_{50} of less than 400 nM (**7u**), and a significant shift from intrinsic to cell-based potency was again observed.

Given the remarkable intrinsic and cell-based potencies associated with **7i**, we made further alterations around the piperazine scaffold. We prepared a number of bridged 2,5-diazabicyclo[2.2.1]heptane analogs **10a**–**10l** and 3,8-diazabicyclo[3.2.1]octane analogs **11a** and **11b** (Tables 5 and 6).

While a number of the bridged analogs showed comparable or improved intrinsic potencies to **7i** as exemplified by **10c**, **10f**, **10g**, **10k**, **10l**, and **11b** none of the bridged analogs showed an improved cell-based potency compared to **7i** with GI_{50}s ranging from 2262 nM (**10l**) to 229 nM (**10f**).

We also prepared a wide variety of bicyclic amino nicotinamides **12a**–**12e** including tetrahydroimidazo[1,2-a] pyrazine analogs, 2,5-diazabicyclo[4.2.0]octane derivatives,

Table 5. In vitro characterization of representative 2,5-diazabicyclo[2.2.1]heptane nicotinamides

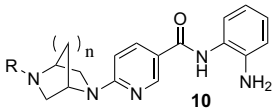

Compound	Method	R	*n*	HDAC1 IC_{50} (nM)[a]	HCT116-72h GI_{50} (nM)[a]
10a	A[i]	H	1	307	—
10b	B	Boc	1	189	282
10c	A[ii]	CBz	1	68	284
10d	A[i]	Bn	1	235	1273
10e	A[ii]	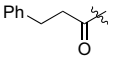	1	167	1480
10f	A[i]	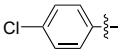	1	39	229
10g	A[i]	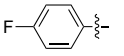	1	54	477
10i	A[i]	H	2	405	—
10j	B	Boc	2	669	7246
10k	A[ii]	CBz	2	67	1510
10l	A[ii]	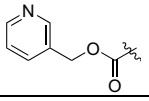	2	91	2262

[a] Values are reported as an average for $n = 2$ or greater.

Table 6. In vitro characterization for a number of 3,8-diazabicyclo[3.2.1]octane nicotinamides

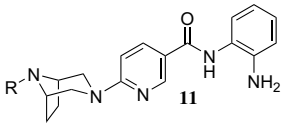

Compound	Method	R	HDAC1 IC_{50} (nM)[a]	HCT116-72h GI_{50} (nM)[a]
11a	B	Boc	167	2581
11b	A[i]	CBz	82	1034

[a] Values are reported as an average for $n = 2$ or greater.

and 1,2,3,4-tetrahydroquinoxalines (Table 7). The most notable of the bicyclic analogs was **12e** with enzymatic activity of 92 nM and HCT116 growth inhibition of 609 nM. Having extensively derivatized the piperazine moiety of the nicotinamide scaffold, we determined that **7i** was a unique 6-amino nicotinamide HDAC inhibitor with excellent intrinsic potency and remarkable cell-based potency worthy of further evaluation in vivo.

Because class I and class II HDACs have very different biological and functional roles, a significant effort has been invested in designing inhibitors that exhibit an improved class I selectivity over inhibiting class II HDACs.[17] The potency and subtype selectivity of **7i** were measured in vitro by monitoring the deacetylation of a synthetic acetyl-lysine bearing peptide by subtype-specific HDAC complexes purified from mammalian cells overexpressing recombinant enzyme.[13] Nicotinamide **7i** showed modest selectivity for HDAC1 over HDAC2, a 13-fold selectivity for HDAC1 over HDAC3, was essentially inactive against HDAC6, and a greater than 225-fold selectivity for HDAC1 over HDAC8 (Table 8). Further in vivo evaluation of **7i** will be necessary to determine what therapeutic advantages class I selectivity offers over less selective HDAC inhibitors.

Table 7. In vitro characterization of representative bicyclic nicotinamides

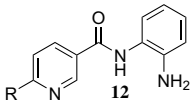

12

Compound	Method	R	HDAC1 IC_{50} (nM)[a]	HCT116-72h GI_{50} (nM)[a]
12a	A[i]	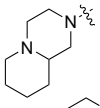	588	723
12b	A[i]	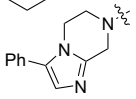	139	1118
12c	A[i]	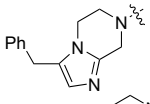	222	866
12d	A[i]	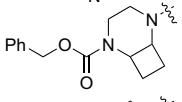	140	3360
12e	B[b]	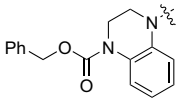	92	609

[a] Values are reported as an average for $n = 2$ or greater.

[b] Method B modification: the pyridyl chloride displacement in this case required using 12 mol % $Pd[P(t\text{-}Bu)_3]_2$ and K_3PO_4 (3 equiv) in PhMe at 85 °C over the course of 12 h.

A homology model of hHDAC1 was built using the crystal structures of human HDAC8 co-crystallized with trichostatin A (PDB entry 1T64)[18] and HDLP co-crystallized with SAHA (PDB entry 1C3S)[19] as templates (Fig. 4).[20] Superposition with the hHDAC8 crystal structure permitted a direct copy of the Zn and select waters into the hHDAC1 homology model. Side-chain torsions of the residues proximate to the Zn were adjusted to reflect those observed in hHDAC8. A set of 150 energy minimized conformers were docked into the hHDAC1 homology model via rigid body alignment such that the aniline NH_2 group and nicotinamide carbonyl approximate the position of the hydroxamate hydroxyl group and hydroxamate carbonyl, respectively, from trichostatin A as observed in the hHDAC8 crystal structure.[21] The remainder of each structure was allowed to access the solvent exposed surface via the ~11 Å channel which provides access to the catalytic Zn. A set of 25 of these conformers were selected for further study based on their ability to uniquely explore various structural features of the homology model without encountering extreme steric clashes with the enzyme model atoms. Each was energy minimized within the context of the hHDAC1 homology model. Residues falling within 10 Å of each conformer were held rigid while side-chains of residues within 5 Å of the compound were energy minimized in conjunction with the inhibitor.

The model shown is the conformer which had the most stabilizing interactions with the enzyme while encountering the least amount of strain relative to its original, ex-enzyme energy minimized state (Fig. 5). Given the vagaries of homology modeling and the approximations made to complete these studies, several other conformers nearly isoenergetic with that presented were retained to provide a more realistic picture of the conformational space which could be sampled by inhibitor **7i**.[22]

In our proposed model, the inhibitor's nicotinamide carbonyl oxygen makes a direct interaction with the Zn 2.4 Å away (Fig. 5). In the case of the template structures HDLP/SAHA and HDAC8/trichostatin, the distance between the hydroxamate carbonyl and Zn is 2.7 and 2.2 Å, respectively. The aniline NH_2 forms a tetrahedral pucker such that the protons form hydrogen bonds with His-140 and His-141 while the nitrogen lone pair interacts with the Zn 2.4 Å away. Relative to the templates HDLP/SAHA and HDAC8/trichostatin, the distance between the hydroxamate oxygen and Zn is 1.8 and 2.2 Å, respectively.

Further removed from the catalytic Zn are two more notable changes which occur during the minimization

Table 8. HDAC In vitro selectivity profile for **7i**

HDAC1 IP (nM)[a]	HDAC2 IP (nM)[a]	HDAC3 IP (nM)[a]	HDAC6 IP (nM)[a]	HDAC8 IP (nM)[a]
73	272	939	>50,000	16,720

[a] Values are reported as an average for $n = 2$ or greater.

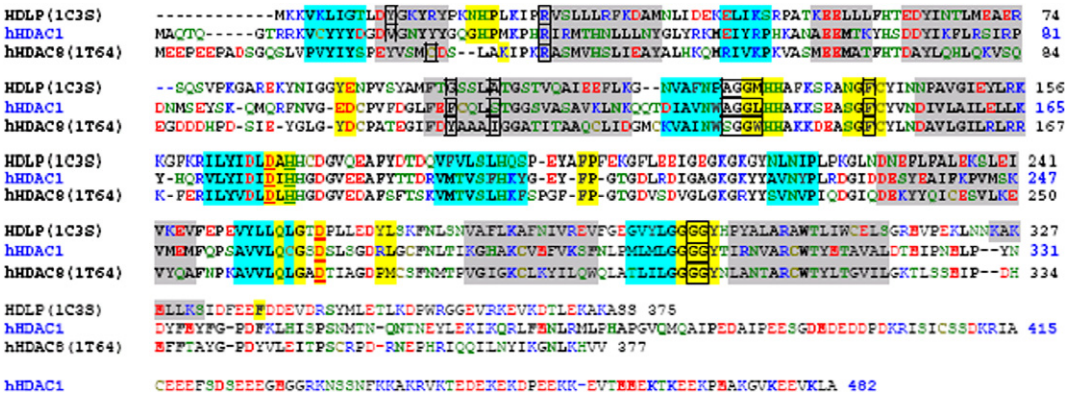

Figure 4. Sequence alignment constructed for HDAC1 homology model.

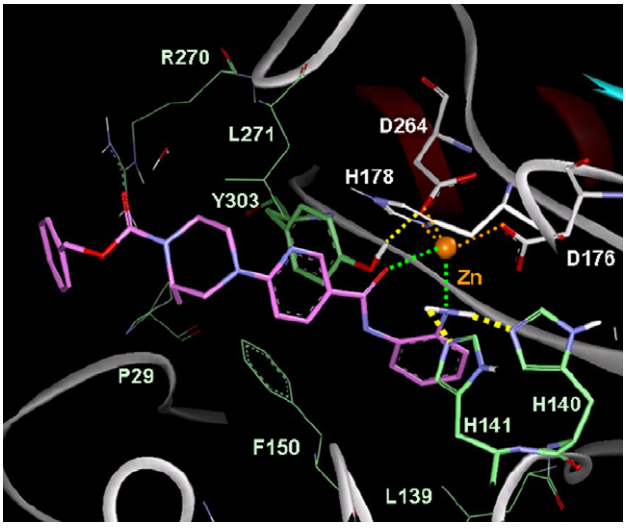

Figure 5. A proposed binding mode for benzamide inhibitor **7i** (purple) in context of the hHDAC1 homology model. The coordination (green and orange dashed lines) between Zn, inhibitor **7i**, and key amino acid residues (white), as well as proposed hydrogen-bonding (yellow dashed lines) are shown.

process. One of these is that the phenolic hydroxyl of Tyr-303 is directed toward the carboxylate of Asp-264 rather than to the nicotinamide carbonyl unlike the observed interaction between the Tyr-OH and hydroxamate carbonyl in the current HDAC/HDLP crystallographic complexes. The other change noted is that the phenyl group of Phe-150, located in the channel, rotates about its axis during minimization such that it is orthogonal to the starting position. This more closely approximates the analogous Phe torsion observed in the HDLP structure rather than that seen in the hHDAC8 structure. The rotation appears to result from the proximity of the nicotinamide amide N–H with which it appears to be forming an edge-to-face π-stacking interaction.

The nicotinamide pyridine and linked piperazine of the inhibitor are modeled to extend through the channel to the solvent exposed region of the enzyme. In the conformer depicted, the pyridine joins the piperazine ''chair'' conformation in an axial fashion which permits the benzyl carbamate to more closely follow the contours of the protein surface. The piperazine is proximate to the Leu-271 side-chain and the methyl substituent descends axially toward Phe-150. The benzyl group approaches Pro-29. In some of the conformers which are nearly isoenergetic with that presented, the piperazine and pyridine are equatorially joined and the carbamate is axially positioned off the piperazine nitrogen. The selectivity observed for HDAC1 over HDAC8 can best be explained in a structural context given that Trp-141 of HDAC8 (Leu-139 for HDAC1) partially occludes the pocket into which the aniline ring of compound **7i** is docked in the HDAC1 homology model.

Having identified **7i** as our lead nicotinamide, we evaluated its pharmacokinetic parameters in 2 species, Sprague–Dawley rat and beagle dog (Table 9). Intravenous dosing in rat (2 mg/kg) led to a moderate clearance and low equilibrium volume of distribution, while oral dosing (4 mg/kg) gave acceptable exposure, oral bioavailability of 32%, and a terminal plasma elimination half-life of 2.2 h. Intravenous dosing in dog (0.9 mg/kg) gave a low clearance as well as a low equilibrium volume of distribution, while oral dosing (1.8 mg/kg) led to high exposure, oral bioavailability of 73%, and a terminal plasma elimination half-life of 5.3 h.

Continuous treatment of HCT116 colon carcinoma cells for 24 h with **7i** resulted in a concentration-dependent hyperacetylation of histone H2B (H2BK5) with an EC_{50} of 2.7 μM, and was accompanied by caspase-3,7 activation consistent with an induction of apoptosis and cell death. It is important to note that histone acetylation at lysine-5 of histone H2B (H2BK5) induced by benzamide **7i** in HCT116 cells was observed within 1 h of treatment and was sustained for more than 8 h after the drug was washed from the cells. Treatment of HCT116 cells with vorinostat for 1 h also resulted in significant H2BK5 acetylation, however this effect was not sustained and diminished rapidly following removal of inhibitor.[23]

The overall ancillary pharmacology profile of **7i** was evaluated to establish if there was any significant off-target activity or other metabolic liabilities associated with the compound. Nicotinamide **7i** was inactive in our

Table 9. Pharmacokinetics profile for **7i**

Species	*n*	IV Dose (mg/kg)	Cl (mL/min/kg)	V_{d}ss (L/kg)	p o Dose (mg/kg)	AUC(N) (μM h kg/mg)	*F* (%)	*t*1/2 (h)
Rat	3	2.0	52	2.1	4.0	0.23	32	2.2
Dog	3	0.9	7.3	2.1	1.8	3.7	73	5.3

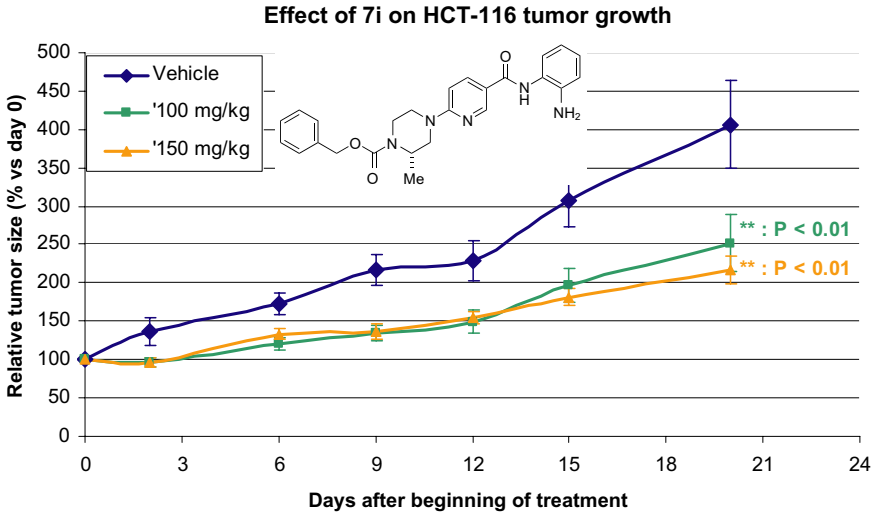

Figure 6. Compound **7i** dosed IP achieves in vivo efficacy in HCT116 tumor bearing mice compared to vehicle (10% DMSO/45% PEG-400/45% water).

hERG binding assay with a $k_i > 30$ μM, which does not predict a liability for **7i** to cause drug-induced QT prolongation. The CYP inhibition potential of **7i** was measured against a number of human isoforms. Nicotinamide **7i** was inactive against CYP3A4 and CYP2D6 with an $IC_{50} > 50$ μM, and showed marginal activity against CYP2C9 with an IC_{50} of 24.5 μM and therefore is not a reversible inhibitor of these major isoforms. In a broad-based biochemical assay screen to check for off-target activities, **7i** exhibited minor activity against human serine/threonine kinase MAPK3 with an $IC_{50} = 4.52$ μM, human dopamine transporter (DAT) with an $IC_{50} = 3.12$ μM, and human serotonin transporter (SERT) with an $IC_{50} = 1.68$ μM.

In a 21-day efficacy study in HCT116 tumor bearing mice, once daily intraperitoneal (IP) administration of **7i** at both 100 mg/kg and 150 mg/kg was well tolerated and inhibited tumor growth by 49% and 53%, respectively, compared with vehicle (Fig. 6). At 7 h post-treatment with **7i**, a mean tumor concentration of 6.0 μM was observed at the 150 mg/kg dose and a mean plasma concentration of 1.8 μM was observed, while at 26 h, a mean tumor concentration of 1.2 μM was observed and a mean plasma concentration of 0.31 μM was observed.

The pharmacokinetics profile and sustained pharmacodynamics of **7i**, coupled with its ancillary pharmacology and established in vivo efficacy, support further investigation of this compound as a potential cancer therapeutic and compare favorably to HDAC inhibitors currently in development.[24]

In summary, we have discovered a series of 6-amino nicotinamides as HDAC inhibitors that possess excellent enzymatic inhibitory activity and cell-based potency. An extensive SAR campaign led to the discovery of 6-amino nicotinamide **7i**, a class I selective inhibitor that possesses remarkable anti-proliferative effects in two cell cultures, displays sustained histone acetylation in vitro, and achieves in vivo efficacy in HCT116 tumor bearing mice. The selectivity profile and cell-based potency for **7i** are most notable for an HDAC inhibitor in the benzamide structural class and further in vivo evaluation of **7i** will determine if these characteristics lead to greater tolerability and efficacy compared to other HDAC inhibitors under clinical investigation. In general, further clinical evaluation of class I selective HDAC inhibitors is needed to determine the therapeutic advantages that greater selectivity might offer with regard to improved tolerability and efficacy compared to less selective HDAC inhibitors already under clinical investigation.

References and notes

1. (a) Feinberg, A. P.; Vogelstein, B. *Nature* **1983**, *301*, 89; (b) Holliday, R. *Science* **1987**, *238*, 163; (c) Jones, P. A.; Baylin, S. B. *Nat. Rev. Genet.* **2002**, *3*, 415.
2. Kouzarides, T. *EMBO J.* **2000**, *19*, 1176.
3. Grozinger, C. M.; Schreiber, S. L. *Chem. Biol.* **2002**, *9*, 3.
4. Urnov, F. D.; Wolffe, A. *Emerg. Ther. Targets* **2000**, *4*, 665.
5. (a) Ng, H. H.; Bird, A. *Trends Biochem. Sci.* **2000**, *25*, 121; (b) Strahl, B. D.; Allis, C. D. *Nature* **2000**, *403*, 41; (c) Jenuwein, T.; Allis, C. D. *Science* **2001**, *293*, 1074.

6. (a) Monneret, C. *Eur. J. Med. Chem.* **2005**, *40*, 1; (b) Kelly, W. K.; O' Connor, O. A.; Marks, P. A. *Expert Opin. Invest. Drugs* **2002**, *11*, 1695.
7. (a) Miller, T. A.; Witter, D. J.; Belvedere, S. *J. Med. Chem.* **2003**, *46*, 5097; (b) Miller, T. A. *Expert Opin. Ther. Pat.* **2004**, *14*, 791.
8. (a) Richon, V. M.; Sandhoff, T. W.; Rifkind, R. A.; Marks, P. A. *Proc. Natl. Acad. Sci. U.S.A.* **2000**, *97*, 10014; (b) Marks, P. A.; Richon, V. M.; Breslow, R.; Rifkind, R. A. *Curr. Opin. Oncol.* **2001**, *13*, 477; (c) Marks, P. A.; Rifkind, R. A.; Richon, V. M.; Breslow, R. *Clin. Cancer Res.* **2001**, *7*, 759; (d) Marks, P. A.; Rifkind, R. A.; Richon, V. M.; Breslow, R.; Miller, T.; Kelly, W. K. *Nat. Rev. Cancer* **2001**, *1*, 194; (e) Meinke, P. T.; Liberator, P. *Curr. Med. Chem.* **2001**, *8*, 211; (f) Marks, P. A.; Miller, T.; Richon, V. M. *Curr. Opin. Pharmacol.* **2003**, *3*, 344; (g) Curtin, M.; Glaser, K. *Curr. Med. Chem.* **2003**, *10*, 2373.
9. (a) Marks, P. A.; Breslow, R. *Nat. Biotechnol.* **2007**, *25*, 84; (b) Kelly, W. K.; O'Connor, O. A.; Marks, P. A. *Expert Opin. Invest. Drugs* **2002**, *11*, 1695; (c) Jenuwein, T.; Allis, C. D. *Science* **2001**, *293*, 1074.
10. (a) Suzuki, T.; Ando, T.; Tsuchiya, K.; Fukazawa, N.; Saito, A.; Mariko, Y.; Yamashita, T.; Nakanishi, O. *J. Med. Chem.* **1999**, *42*, 3001; (b) Saito, A.; Yamashita, T.; Mariko, Y.; Nosaka, Y.; Tsuchiya, K.; Ando, T.; Suzuki, T.; Tsuruo, T.; Nakanishi, O. *Proc. Natl. Acad. Sci.* **1999**, *96*, 4592; (c) Jaboin, J.; Wild, J.; Hamidi, H.; Khanna, C.; Kim, C. J.; Robey, R.; Bates, S. E.; Thiele, C. J. *Cancer Res.* **2002**, *62*, 6108.
11. (a) El-Beltagi, H. M.; Martens, A. C. M.; Lelieveld, P.; Haroun, E. A.; Hagenbeek, A. *Cancer Res.* **1993**, *53*, 3008; (b) Loprevite, M.; Tiseo, M.; Grossi, F.; Scolaro, T.; Semino, C.; Pandolfi, A.; Favoni, R.; Ardizzoni, A. *Oncol. Res.* **2005**, *15*, 39; (c) Foster, B. J.; Jones, L.; Wiegand, R.; Lorusso, P. M.; Corbett, T. H. *Invest. New Drugs* **1997**, *15*, 187.
12. (a) Delorme, D.; Woo, S. H.; Vaisburg, A.; Moradel, O.; Leit, S.; Raeppel, S.; Frechette, S.; Bouchain, G. *PCT Int. Appl.* **2003**, WO 2003024448; (b) Siu, L. L; Carducci, M.; Pearce, L.; Maclean, M.; Sullivan, R.; Li, Z.; Kalita, A.; Chen, E. X.; Pili, R.; Longstreth, J.; Martell, R. E.; Reid, G. K. *Abstracts of Posters, C77: Phase I Study of Isotype Selective Histone Deactylase (HDAC) Inhibitor MGCD0103 Given as Three-Times Weekly Oral Dose in Patients (pts) with Advanced Solid Tumors*, AACR-NCI-EORTC International Conference on Molecular Targets and Cancer Therapeutics: Discovery, Biology, and Clinical Applications, Philadelphia, Pennsylvania, November 14–18, 2005.
13. The HDAC Fluorescent HDAC1 and HDAC8 Fluor-de-Lys Activity Assays from BioMol Research Laboratories (Plymouth Meeting, PA) provided the basis for our HDAC activity assays. The assay buffer for the HDAC1 and HDAC2 assays consisted of 20 mM Hepes, pH 8.0, 137 mM NaCl, 2.7 mM KCl, 1 mM $MgCl_2$, 0.1 mg/mL BSA; for the HDAC3 assay it was 20 mM Hepes, pH 8.0, 137 mM NaCl, 2.7 mM KCl, 1 mM $MgCl_2$, and 0.25 mg/ml BSA; for the HDAC6 assay, it was 20 mM Hepes, pH 7.4, 137 mM NaCl, 2.7 mM KCl, 1 mM $MgCl_2$, and 0.1 mg/mL BSA; and for the HDAC8 assay, it was 20 mM Hepes, pH 8.0, 100 mM NaCl, 20 mM KCl, 1 mM $MgCl_2$, and 0.1 mg/mL BSA. HDAC enzymatic activities were determined by the following procedure: 3× serial dilutions of a 10 mM solution of inhibitor were performed in DMSO followed by a 20× dilution into Assay buffer. 20 μl HDAC was preincubated with 5 μL diluted compound at RT for 10 min. The reaction was initiated by the addition of 25 μL of the appropriate substrate (HDACs 1, 2, 3, and 6: fluor-de-Lys substrate KI-104; HDAC8: fluor-de-Lys HDAC8 substrate KI-178), incubated 15 (HDAC8) or 60 (HDACs 1, 2, 3, and 6) minutes at 37 °C, before adding 50 μL of the appropriate development solution. The development solution for HDACs 1, 2, 3, and 6 was 167×-diluted 20× Developer Concentrate (BIOMOL: KI-105) plus 10 μM SAHA. For HDAC8, the development solution was 100×-diluted 5× Developer Concentrate (BIOMOL: KI-176) plus 10 μM SAHA. The assay was read in a VictorV plate reader (Perkin-Elmer, Wellesley, MA) at Ex 360 nm/Em 460 nm. The final substrate concentration was 30 μM and final HDAC concentrations in the reaction were 1 nM for HDACs 1, 3, and 6), 2 nM for HDAC2, and 15 nM for HDAC8. Carboxy-terminal FLAG-tagged human HDACs 1, 2, 3 (co-expressed with the domain of SMRT), and 6 were overexpressed in mammalian cells and affinity purified using an anti-Flag antibody matrix, eluted from the matrix with 100 μg/mL of a competing FLAG peptide in 20 mM Tris–Cl, pH 8.0, 150 mM NaCl, 10% glycerol, and protease inhibitor cocktail (Roche cat. # 1836153).
14. Seto, C. T.; Mathias, J. P.; Whitesides, G. M. *J. Am. Chem. Soc.* **1993**, *115*, 1321.
15. HDAC cell-based proliferation results were determined by the following procedure: HCT116 cells were plated in 96-well plates at density of 1000 cells/well. The next day, cells were treated with either 0.2% DMSO or increasing concentrations of **7i** dissolved in DMSO (final concentration DMSO 0.2%). After 72 h incubation at 37 °C with 5% CO_2, viable cells were quantitated using Vialight Plus (Cambrex) according to manufacturer's instructions.
16. Experimental procedure for the synthesis of **7i**: a mixture of the Boc-protected chloronicotinamide (3.0 g, 8.6 mmol) and benzyl-(2*S*)-2-methylpiperazine-1-carboxylate (6.0 g, 25.8 mmol) in PhMe (5 mL) was heated at 85 °C for 12 h. The reaction mixture was diluted with EtOAc (100 mL), and washed with satd aq $NaHCO_3$ (1 × 25 mL) and brine (1 × 25 mL). The crude oil was purified by reverse phase chromatography (25–100% MeCN/H_2O with 0.05% TFA) and formation of the desired Boc-protected piperazinyl nicotinamide was confirmed by LC/MS (ESI+): calcd $[M+H]^+$ 546.3, exp. 546.3. The Boc-protected piperazinyl nicotinamide was treated with TFA (4 mL) in CH_2Cl_2 (8 mL) and after 20 min of stirring at room temperature, the reaction mixture was concentrated and purified by reverse phase chromatography (15–75% MeCN/H_2O with 0.05% TFA). The appropriate fractions were combined, diluted with EtOAc (150 mL) and washed with satd aq $NaHCO_3$ (1 × 50 mL) and brine (1 × 50 mL). The organic layer was dried over Na_2SO_4, filtered, and concentrated to give the desired nicotinamide **7i**: ^1H NMR (600 MHz, DMSO-d_6) δ 9.42 (s, 1H), 8.69 (s, 1H), 8.05 (d, J = 8.8 Hz, 1H), 7.34–7.29 (m, 5H), 7.10 (d, J = 7.3 Hz, 1H), 6.92 (t, J = 7.3 Hz, 1H), 6.85 (d, J = 9.1 Hz, 1H), 6.73 (d, J = 7.9 Hz, 1H), 6.55 (m, 1H), 5.11–4.85 (m, 2H), 4.83 (br s, 2H), 4.26-4.21 (m, 3H), 3.85 (dd, J = 5.0 Hz, 3.5 Hz, 1H), 3.34–3.22 (m, 2H), 3.20–3.00 (m, 1H), 1.07 (d, J = 6.5 Hz, 3H); MS (ESI+): calcd $[M+H]^+$ 446.2, exp. 446.2.
17. (a) Heltweg, B.; Dequiedt, F.; Marshall, B. L.; Brauch, C.; Yoshida, M.; Nishino, N.; Verdin, E.; Jung, M. *J. Med. Chem.* **2004**, *47*, 5235; (b) Curtin, M. L. *Expert Opin. Ther. Pat.* **2002**, *12*, 1375.
18. HDAC8 crystal structure (1T64) Somoza, J. R.; Skene, R. J.; Katz, B. A.; Mol, C.; Ho, J. D.; Jennings, A. J.; Luong, C.; Arvai, A.; Buggy, J. J.; Chi, E.; Tang, J.; Sang, B.-C.; Verner, E.; Wynands, R.; Leahy, E. M.; Dougan, D. R.; Snell, G.; Navre, M.; Knuth, M. W.; Swanson, R. V.; McRee, DE.; Tari, L. W. *Structure* **2004**, *12*, 1325.
19. HDAC8 crystal structure (1T64) (a) Somoza, J. R.; Skene, R. J.; Katz, B. A.; Mol, C.; Ho, J. D.; Jennings, A. J.;

Luong, C.; Arvai, A.; Buggy, J. J.; Chi, E.; Tang, J.; Sang, B.-C.; Verner, E.; Wynands, R.; Leahy, E. M.; Dougan, D. R.; Snell, G.; Navre, M.; Knuth, M. W.; Swanson, R. V.; McRee, DE.; Tari, L. W. *Structure* **2004**, *12*, 1325; HDLP crystal structure (1C3S); (b) Finnin, M. S.; Donigian, J. R.; Cohen, A.; Richon, V. M.; Rifkind, R. A.; Marks, P. A.; Breslow, R.; Pavletich, N. P. *Nature* **1999**, *401*, 188.

20. An alignment of the two crystal structures and the amino acid sequence for hHDAC1 (retrieved from SwissProt, accession ID: Q13547) was accomplished using the sequence/structure alignment tools in MOE (Chemical Computing Group, Montreal, Canada). This alignment was then used in Quanta/Modeler5 (Accelrys, San Diego, CA, USA) to generate a set of homology models. That with the least number of violations was further energy minimized using CHARMm 200 steps steepest descents without the catalytic Zn or any waters present: (a) Sánchez, R.; Sali, A. Comparative protein structure modeling. In *Protein Structure Prediction: Methods and Protocols*; Webster, D. M., Ed.; Humana Press: New Jersey, 2000; Vol. 143, pp. 97–129; (b) Brooks, B. R.; Bruccoleri, R. E.; Olafson, B. D.; States, D. J.; Swaminathan, S.; Karplus, M. *J. Comp. Chem.* **1983**, *4*, 187; (c) Wang, D.-F.; Helquist, P.; Wiech, N. L.; Wiest, O. *J. Med. Chem.* **2005**, *48*, 6936.
21. The 150 conformers were generated and energy minimized using MMFFs with a distance-dependent dielectric of 2*r*: (a) Crippen, C. M.; Havel, T. F. Distance Geometry and Molecular Conformation. In *Chemometrics Research Studies Series*; Bawden, D., Ed.; Research Studies Press, Wiley: New York, 1988; (b) Halgren, T. A. *J. Comp. Chem.* **1999**, *20*, 720.
22. During the course of energy minimization within the context of the enzyme model, only slight differences in the presentation of the co-minimizing residues (those within 5 Å of the inhibitor) were noted between the starting and final enzyme structure. The catalytic Zn and chelating residues were virtually unchanged during the minimization process.
23. Acetylation assays were performed using the following procedures: HCT116 cells were plated in 6-well plates at a density of 1×10^6 cells per well. The next day, cells were incubated at 37 °C, 5% CO_2 for 24 hours with either 0.2% DMSO or increasing concentrations of **7i** dissolved in DMSO (final DMSO concentration = 0.2%). Whole cell lysates were made by disrupting cell membranes with 2% deoxycholate followed by sonication. Using these HCT116 lysates as antigen, H2BK5 acetylation was quantified using an indirect ELISA and normalized to total H2B levels obtained using a second indirect ELISA. Primary antibodies used were rabbit anti-acetylated H2BK5 (Cell Signaling) and sheep anti-histone H2B (Abcam). Goat anti-rabbit IgG HRP (Bio-Rad) and rabbit anti-sheep-HRP (Jackson ImmunoResearch) were used as secondary antibodies, respectively. TMB substrate (Pierce) was used for detection with absorbance read at 450 nm.
24. (a) Yoo, C. B.; Jones, P. A. *Nat. Rev. Drug Disc.* **2006**, *5*, 37; (b) Bolden, J. E.; Peart, M. J.; Johnstone, R. W. *Nat. Rev. Drug. Disc.* **2006**, *5*, 769; (c) Moradei, O.; Maroun, C. R.; Paquin, I.; Vaisburg, A. *Curr. Med. Chem.: Anti-Cancer Agents* **2005**, *5*, 529.